Identification of a bile acid-binding transcription factor in *Clostridioides difficile* using chemical proteomics

Forster ER[1,2], Yang X[3], Hang HC[3,4], Shen A[2]

[1]Graduate School of Biomedical Sciences, Tufts University, Boston MA, USA

[2]Department of Molecular Biology and Microbiology, Tufts University School of Medicine, Boston MA, USA

[3]Department of Immunology and Microbiology, Scripps Research, La Jolla CA, USA

[4]Department of Chemistry, Scripps Research, La Jolla CA, USA

Abstract

Clostridioides difficile is a Gram-positive anaerobic bacterium that is the leading cause of hospital-acquired gastroenteritis in the US. In the gut milieu, *C. difficile* encounters microbiota-derived bile acids capable of inhibiting its growth, which are thought to be a mechanism of colonization resistance. While the levels of certain bile acids in the gut correlate with susceptibility to *C. difficile* infection, their molecular targets in *C. difficile* remain unknown. In this study, we sought to use chemical proteomics to identify bile acid-interacting proteins in *C. difficile*. Using photoaffinity bile acid probes and chemical proteomics, we identified a previously uncharacterized MerR family protein, CD3583 (now BapR), as a putative bile acid-sensing transcription regulator. Our data indicate that BapR binds and is stabilized by lithocholic acid (LCA) in *C. difficile*. Although loss of BapR did not affect *C. difficile*'s sensitivity to LCA, Δ*bapR* cells elongated more in the presence of LCA compared to wild-type cells. Transcriptomics revealed that BapR regulates the expression of the gene clusters *mdeA-cd3573* and *cd0618-cd0616*, and *cwpV*, with the expression of the *mdeA-cd3573* locus being specifically de-repressed in the presence of LCA in a BapR-dependent manner. Electrophoretic mobility shift assays revealed that BapR directly binds to the *mdeA* promoter region. Since *mdeA* is involved in amino acid-related sulfur metabolism and the *mdeA-cd3573* locus encodes putative transporters, we propose that BapR senses a gastrointestinal tract-specific small molecule, LCA, as an environmental cue for metabolic adaptation.

Introduction

Clostridioides difficile is a Gram-positive, anerobic, spore-forming bacterium that is a leading cause of nosocomial gastroenteritis worldwide (1, 2). In 2017, *C. difficile* was responsible for ~460,000 infections and ~13,000 deaths in the United States alone (3). *C. difficile* infections (CDIs) are transmitted by its aerotolerant spores, which germinate in the distal small intestine in response to cholate-derived bile acids, giving rise to toxin-producing vegetative cells that colonize the colon (4). While prior antibiotic use and the consequent disruption of the gut microbiota is a primary risk factor for CDI, the specific mechanisms by which the microbiota protect against CDI remain largely unknown. However, production of secondary bile acids by the gut microbiota has been proposed to be a major contributor to colonization resistance. Bacteria that produce secondary bile acids are sufficient to confer colonization resistance against CDI, and the levels of these secondary bile acids in the gut correlate with resistance to CDI (4–8). Additionally, *C. difficile* is highly sensitive to growth inhibition by secondary bile acids, with lithocholic acid (LCA) and its derivatives being the most potent inhibitors (6, 7, 9).

Bile acids are amphipathic, detergent-like molecules produced by the liver and secreted into the small intestine to aid in fat digestion. Host-derived primary bile acids are largely reabsorbed via enterohepatic recirculation in the distal small intestine, but approximately 5% reach the large intestine where they are transformed into secondary bile acids by the microbiota (10). In cecal samples obtained from individuals who died an unnatural death, total bile acids were measured at ~200 - 1,000 μM (11). This pool consisted mostly of the secondary bile acids LCA and deoxycholic acid (DCA): on average, each represented ~25-33% of the bile acids in the non-CDI cecum (11) and feces (10). Growing evidence suggests that microbiota-derived secondary bile acids have broad pathophysiological implications in the host from carcinogenesis (12) to immune modulation and inflammation (13–20) to pathogen resistance (9, 21, 22), including *C.*

difficile. Indeed, bile acids cause a broad range of stresses in bacteria including membrane disruption, protein denaturation, iron and calcium chelation, and DNA damage (23, 24).

DCA and LCA are made from the primary bile acids cholic acid (CA) and chenodeoxycholic acid (CDCA), respectively, via 7α-dehydroxylation by a select few members of the gut microbiota (25–31). This activity is encoded by the bile acid-inducible (*bai*) operon (25–31), which is highly correlated with resistance to CDI in animal models (7, 30, 31). A few *bai* operon-positive *Clostridium* species, namely *C. scindens*, are each sufficient to protect mice against CDI (7, 32, 33), although *bai* operon mutant strains have not yet been tested presumably due to genetic limitations. Notably, sequestration of bile from the cecal contents of *C. scindens*-colonized mice with cholestyramine is sufficient to rescue *C. difficile* growth *ex vivo*, suggesting that the bile acids produced by *C. scindens* inhibit *C. difficile* infection (7). Further, DCA and LCA are undetectable in the cecal contents of antibiotic-treated mice and recurrent CDI patient feces, but they are present in gut environments that are inhibitory to *C. difficile* (4–6, 8, 34). Underscoring these correlations, concentrations of DCA and LCA present in CDI-resistant mice are sufficient to inhibit *C. difficile* growth *in vitro* (6), and LCA tolerance correlates with virulence across *C. difficile* strains in a murine model of infection (35). While subsequent studies suggest that 7α-dehydroxylating bacteria also inhibit *C. difficile* through bile acid-independent mechanisms such as antibiotic production and competition for Stickland metabolism substrates (32, 36), secondary bile acids nonetheless appear to be a major contributor.

Gut commensals and several gut pathogens have evolved mechanisms to resist or tolerate the toxicity of bile acids (23, 24, 37), yet resistance mechanisms remain undefined in *C. difficile*. Currently, little is known about *C. difficile*'s interactions with bile acids at the molecular level, although bile acids have been shown to modulate several aspects of *C. difficile* physiology. LCA causes loss of flagella and cell elongation (38) whereas DCA induces biofilm formation and represses sporulation (39). Toxin expression and/or activity is inhibited by LCA, DCA, isolithocholic acid (isoLCA), isodeoxycholic acid, and ursodeoxycholic acid, and the TcdB toxin

was recently shown to bind several bile acids (39–41). This latter observation represents the sole biochemical evidence of a *C. difficile* protein specifically binding to a bile acid to date. Indeed, while genetic studies suggest that the CspC pseudoprotease is a receptor for the primary bile acid germinant, taurocholic acid (TCA) (42), direct binding of TCA or other cholate-derived bile acid germinants (43) to *C. difficile* spore proteins has not been demonstrated. Furthermore, no targets of bile acids in *C. difficile* vegetative cells have been identified.

In this study, we employed recently developed photoaffinity bile acid probes in a chemical proteomics screen to identify the targets of toxic bile acids in vegetative *C. difficile*. While our screen identified several essential proteins as targets of LCA-derived probes, a putative MerR family transcription factor, CD3583 (now BapR), was highly enriched. Here, we demonstrate that BapR binds to LCA in *C. difficile*. BapR appears to modulate cell length in response to LCA and directly represses the expression of a locus encoding genes involved in sulfur metabolism. Our data also indicate that BapR indirectly represses the expression of two additional loci encoding two other putative transcription factors and the cell wall protein CwpV.

Results

Bile acid probes label distinct *C. difficile* proteins in a dose-dependent manner

Coupling photoaffinity probes of microbiota metabolites with chemical proteomics affords new opportunities to characterize specific protein targets and elucidate small molecule mechanisms of action (44). For example, bile acid photoaffinity probes recently identified the HilD regulator of SPI-1 virulence gene expression as a target of CDCA in *Salmonella* Typhimurium (Yang X, Stein K, Hang HC in revision). Using a similar approach, we sought to uncover the targets of bile acids in *C. difficile* to gain insight into the mechanism of inhibition by DCA or LCA and potential

adaptation of *C. difficile* to these toxic, microbiota-derived molecules. These probes are generated from naturally occurring bile acids with the addition of two functional groups for photocrosslinking and bioorthogonal detection (**Figure 1A**). The diazirine functional group allows for covalent crosslinking to interacting proteins using UV light, while the terminal alkyne tag allows for detection or isolation of interacting proteins after bioorthogonal labeling with fluorophore-azide or biotin-azide reagents, respectively (**Figure 1B**).

To gain insight into how toxic bile acids affect *C. difficile*'s physiology, we sought to identify targets of these microbiota-derived molecules. Since LCA potently inhibits growth of *C. difficile*, we employed LCA-derived probes to identify LCA's cellular targets. Using growth inhibition in broth culture as a readout of probe activity, we found that Probe 8 potently inhibited growth with an IC_{50} of ~10 μM (**Figure 1C**). This inhibition was comparable to the IC_{50} of isoallolithocholic acid (isoalloLCA, ~2 μM, **Figure 1D**), which was recently identified as an especially toxic bile acid to *C. difficile* in the gut of centenarians (9). Although solubility limited the range of concentrations we could test, Probe 8 was more potent than LCA (IC_{50} ~50 μM) and DCA and CDCA (IC_{50}s of ~100 μM, **Figure 1D and Figure S2**). The primary bile acids CA and TCA did not inhibit growth up to 400 μM (**Figure 1D and Figure S2**). Importantly, we observed these effects at physiologically relevant concentrations since LCA and DCA have been measured at 1 - 450 μM and 30 - 700 μM, respectively, in non-CDI human cecal contents (11) and ~1 mM and ~1.2 mM, respectively, in human feces post-FMT (34). Interestingly, Probe 3 did not appreciably inhibit the growth of *C. difficile* (**Figure 1C**) despite sharing LCA as a parent structure with Probe 8. Due to its structural similarity to Probe 8 yet substantially reduced growth inhibitory activity, we selected Probe 3 as a control probe.

To qualitatively assess whether the probes specifically interact with proteins in *C. difficile*, we used fluorescent SDS-PAGE to visualize labeling. To this end, we treated log-phase *C. difficile* cultures with 2.5 or 25 μM Probe 8 or DMSO vehicle for 30 minutes, washed cells to remove unbound probe, and UV irradiated cells to covalently link the probe to interacting proteins. After

generating total cell lysate and performing a click reaction in the total lysate to conjugate AlexaFluor-488-azide to the probe, these probe-bound proteins were visualized by SDS-PAGE using fluorescent imaging (**Figure 1B**). We observed distinct bands in a dose- and UV-dependent manner indicative of Probe 8 interacting with specific *C. difficile* proteins (**Figure 1E**). Possibly in line with its reduced growth inhibitory activity, Probe 3 exhibited weaker labeling (**Figure S1**).

Chemical proteomics identifies bile acid-binding proteins in *C. difficile*

To identify the direct targets of Probe 8 visualized in the in-gel fluorescence assay, we used a chemical proteomics approach to enrich for probe-bound proteins. After conjugating biotin-azide onto probe-bound proteins (**Figure 1B**), we used streptavidin beads to isolate the proteins that interacted with Probe 8 and/or Probe 3 after 1 hour of treatment during log-phase (**Figure S1**). Streptavidin-enriched proteins were then identified using label-free quantitative liquid chromatography-tandem mass spectrometry (**Figure 1F and Table S1**). These proteomic analyses revealed 48 hits for Probe 8 and 52 hits for Probe 3 relative to DMSO (modified Z score > 3). Of the Probe 8 hits, 27 were specific to Probe 8 over Probe 3 (**Figure 1G**). We were particularly interested in Probe 8-specific proteins because Probe 8 is associated with growth inhibitory activity. Consistent with the toxicity of Probe 8 and its parent LCA molecule, 9 of the 27 hits specific to Probe 8 were essential (45). These included proteins involved in DNA replication, transcription, or cell division, namely DnaA, NusA, and MinD. The coenzyme A synthesis protein CoaBC and fatty acid synthesis protein FabD were additional essential hits. The essential cell wall synthesis protein MurC was of particular interest considering that *C. difficile* cells elongate with LCA treatment (38). However, the most enriched protein from our screen was a non-essential MerR family transcription factor, CD3583 (herein bile acid-binding protein regulator BapR; locus tag CD630_35830) (**Figure 1F**). MerR family transcription factors typically regulate efflux pumps that export the toxic molecules they sense (46) and can function as repressors in the absence of

ligand as well as activators upon ligand binding. Given the role of MerR family transcription factors in regulating resistance or adaptative responses, we sought to explore the function of BapR in *C. difficile*.

BapR specifically binds LCA-derived bile acids

Structural modeling using iTASSER (47) predicted that BapR is highly similar to a MerR family transcription factor in *Bacillus subtilis*, BmrR. BapR shares 18% identity and 28% similarity with BmrR, most of which is in the N-terminal region. MerR family transcription factors have conserved N-terminal DNA binding domains and variable C-terminal ligand-binding domains. These ligand binding domains have been observed to sense and respond to a wide diversity of molecules, with ligands ranging from metal ions to large amphipathic drugs (48). Although BmrR does not bind bile acids, its ligands are large hydrophobic molecules with some similarity to the sterol center of bile acids (49–51).

To validate BapR as a target of Probe 8, we used an independent method for assessing whether the bile acid probes could pull down BapR from *C. difficile*. Specifically, we treated *C. difficile* cultures expressing a FLAG-tagged allele of *bapR* from its native locus with either DMSO, Probe 8, or Probe 3 for 1 hour during log-phase. The probe was UV crosslinked to its protein targets, and then the cells were lysed. After conjugating biotin-azide to probe-bound proteins using click chemistry, we isolated these proteins using streptavidin beads (**Figure 1B**). FLAG-tagged BapR was enriched in the pull-downs using Probe 8, and to a lesser extent using Probe 3, relative to DMSO-treated cultures (**Figure 2A**, representative of three biological replicates). More biotinylated probe-bound protein was present in the Probe 8 pull-downs relative to Probe 3 as detected with fluorescent streptavidin, consistent with Probe 8 interacting with more proteins in our proteomics screen (**Figure 1F and Table S1**).

To determine whether we could directly detect binding between BapR and LCA, we used thermal shift assays to compare the relative affinity of BapR for different bile acids. Thermal shift assays (also known as differential scanning fluorimetry, DSF) measure the change in melting temperature (T_m) of a protein in the presence of a ligand using a fluorescent dye that binds to hydrophobic regions of a protein as it unfolds. While ligand binding typically increases the T_m of a protein because ligand binding stabilizes proteins, it can in some instances decrease the T_m if the conformation stabilized by the ligand melts more readily (52). An example of this phenomenon can be found in isoLCA binding to the eukaryotic AKR1A1 aldo-keto reductase, for which isoLCA is a known ligand (53). Like AKR1A1, we observed a dose-dependent decrease in T_m when purified BapR (**Figure 2C**) was incubated with increasing concentrations of Probe 8 and certain bile acids in the presence of SYPRO Orange dye (**Figure 2D and E**). Specifically, we detected a ~4˚C T_m shift with 32 μM Probe 8 compared to a ~1˚C T_m shift with Probe 3 at the same concentration. We also observed up to a ~5˚C T_m shift at 64 μM LCA, whereas DCA and CDCA required ~10-fold higher concentrations (500 μM) to shift the T_m of BapR by ~3˚C. Furthermore, CA and TCA were only able to shift the T_m by ~1-2˚C at 2 mM. It should be noted that the maximum concentration shown for each ligand tested was limited by measuring the non-specific interactions of a given bile acid with the SYPRO Orange dye (i.e. in the absence of BapR).

The apparent affinity of BapR for specific bile acids (LCA > DCA/CDCA > CA/TCA) correlates with fewer hydroxyl groups on the α face of the steroid center (**Figure 2B**), suggesting that hydrophobicity of the bile acid influences it interaction with BapR. IsoalloLCA differs from LCA in the orientation of the 3-OH and most notably by the stereochemistry at carbon 5: the 5β hydrogen in LCA results in a “bent” steroid ring, whereas the 5α hydrogen in isoalloLCA results in a more planar conformation. Interestingly, BapR appeared to have higher affinity for isoalloLCA given that it induced a ~5˚C T_m shift at a 2-fold lower concentration than LCA (32 μM vs. 64 μM, **Figure 2E**). The hydroxyl at carbon 3 is on the β face of the steroid center of isoalloLCA opposed

to the α face for LCA, further implying that hydrophobicity of the α face is important for interaction with BapR.

BapR influences cell length and interacts with LCA in *C. difficile*

After confirming that BapR binds bile acids, we sought to determine the physiological function of BapR in *C. difficile*. We initially hypothesized that BapR regulates resistance to bile acids like other MerR family transcription factors that regulate resistance to their ligands (48). However, we were unable to detect a growth defect for *C. difficile* lacking *bapR* in the presence of LCA (**Figure 3A**) or isoalloLCA (**Figure S3**). Besides growth inhibition, cell elongation and loss of flagella are the only known effects of LCA on *C. difficile* (38), so we instead asked whether BapR influences these phenotypes. While BapR did not influence motility on soft agar (data not shown), we observed that loss of BapR resulted in cells elongating ~25% more than wild-type (WT) cells after a 3-hour exposure to 20 μM LCA (**Figure 3B**). Specifically, although LCA treatment increased the length of WT *C. difficile* cells by ~2 μm, Δ*bapR* cells elongated an additional ~0.5 μm over the WT strain under these conditions (**Figure 3C**). This phenotype was complemented by expressing *bapR* from its native promoter at the ectopic *pyrE* locus on the chromosome (Δ*bapR*/*bapR*; **Figure 3C**) (54). We did not observe gross morphological differences aside from cell length between the strains upon LCA exposure.

To gain initial mechanistic insight into BapR's response to bile acids in *C. difficile*, we asked whether *bapR* expression changes during bile acid-mediated stress. To this end, we measured *bapR* transcript levels by qRT-PCR after 1-hour exposure to 20 μM LCA or DMSO vehicle during log-phase. Expression of *bapR* decreased ~3-fold in the WT strain upon LCA treatment (*bapR* transcript was undetectable in the Δ*bapR* strain as expected) (**Figure 4A**). Despite the unanticipated overexpression of *bapR* in the Δ*bapR*/*bapR* complement strain, *bapR* expression was down-regulated upon treatment of these cells with LCA (**Figure 4A**).

Since our finding that *bapR* expression decreased in response to LCA was somewhat surprising, we wondered whether this decrease corresponded to lower protein levels. To test this possibility, we treated log-phase *C. difficile* cultures with increasing concentrations of LCA, DCA, CDCA, TCA, or isoalloLCA for 3 hours during log-phase and assessed BapR levels by Western blot. Unexpectedly, we observed a dose-dependent increase in BapR levels with LCA, and to a lesser extent with DCA, CDCA, and isoalloLCA (**Figure 4B and C**). This implies that BapR is stabilized by these bile acids or becomes less susceptible to degradation in *C. difficile*, since *bapR* transcript levels are decreased upon LCA treatment (**Figure 4A**). The elevated BapR levels were sustained for at least 6 hours of growth with LCA (**Figure S4**). In agreement with the apparent binding affinity measured in thermal shift assays, ~10-fold higher concentrations of DCA and CDCA were needed to stabilize BapR at levels comparable to LCA (~3-fold increase at 50 μM LCA vs. ~2-fold increase at 500 μM DCA or CDCA). TCA did not change BapR levels even at 500 μM, and since BapR did not appreciably bind TCA in our thermal shift assays, the elevated BapR levels in *C. difficile* seen upon treatment with the other bile acids is likely due to binding. It is unclear why isoalloLCA increased BapR levels less than LCA in WT *C. difficile* and more in the complementation strain, but these data nevertheless suggest that BapR interacts with bile acids in *C. difficile*.

BapR controls gene expression, in some cases in an LCA-dependent manner

Since BapR is predicted to be a MerR-type transcription factor, we next asked whether it regulates gene expression, particularly in an LCA-dependent manner. To this end, we assessed the transcriptome of WT and Δ*bapR C. difficile* during short-term LCA exposure using RNA-seq. Log-phase cultures of each strain were treated with 20 μM LCA or DMSO vehicle for 1 hour before harvesting RNA for next-generation sequencing. Transcriptomic analysis revealed that LCA induced global changes in gene expression (569 genes significantly upregulated and 580 genes

significantly downregulated; $p < 0.05$ and fold change > 2) (**Figure S5A** and **Table S2**). We noted changes in line with previously reported effects of LCA on *C. difficile*: motility genes were largely downregulated in our analyses, consistent with LCA causing loss of flagella (38) (**Figure S5B**). While the expression of many genes was altered by LCA, we were most interested in genes whose expression was modulated in a BapR-dependent manner. We found that BapR significantly influenced the expression of three gene loci: *mdeA-cd3576* (CD630_35770-CD630_35760), *cd0618-cd0616* (CD630_06180-CD630_06160), and *cwpV* (CD630_05140) (**Figure 5A**). Expression of these genes was higher in the Δ*bapR* strain relative to WT (2-4-fold different), indicating that BapR represses them.

Of the genes significantly affected by BapR, *mdeA* and *cd3576* expression changed the most between DMSO and LCA conditions. These genes were differentially expressed in the DMSO control (WT vs. Δ*bapR*) but not in the presence of LCA (**Figure 5A**). *mdeA* encodes a methionine γ-lyase thought to be responsible for methanethiol and H_2S production from methionine and homocysteine/cysteine, respectively, (55). *cd3576* encodes a major facilitator superfamily (MFS) transporter. These genes are found in close proximity to the upstream genes, *cd3575-cd3573* (**Figure 5B**), which are predicted to encode two hypothetical proteins and a sodium:solute symporter, respectively. While genome-wide transcription start site (TSS) mapping in *C. difficile* predicts promoters at *cd3578* and *cd3571*, no TSSs were reported for *mdeA-cd3572* (56) (**Figure 5B**), although in our experience these genome-wide analyses do not capture all TSS. Since *cd3573-cd3575* approached significance under at least one condition (*cd3572* and *cd3578* did not) and may be co-transcribed with *cd3576* and *mdeA* based on proximity and orientation, we validated expression of *mdeA-cd3573* using qRT-PCR. In line with our RNA-seq analyses, we found that all genes in this cluster were expressed more in the Δ*bapR* strain than WT under both conditions, and the differential expression was complemented in the Δ*bapR*/*bapR* strain (**Figure 5C**). Additionally, LCA increased the expression of all genes in the cluster across all strains (**Figure 5C**). To compare the response to LCA between strains, we plotted expression levels for

a given strain as the fold-change in LCA relative to DMSO (LCA/DMSO). This revealed that the loss of BapR resulted in a smaller induction of these genes in the presence of LCA relative to WT levels (**Figure 5D**); the differential response was most apparent for *mdeA* and *cd3576* (~6-fold induction in the WT and complement strains vs. ~1.5-fold induction in the Δ*bapR* strain). Taken together these data suggest that BapR is necessary to induce these genes in response to LCA, likely by de-repressing their expression upon sensing LCA.

In contrast, *cwpV*, which was differentially expressed between Δ*bapR* and WT *C. difficile* in our RNA-seq analyses, was not affected by LCA treatment (**Figure 5A**). CwpV is a cell wall protein that makes up ~13% of the total surface layer proteins in *C. difficile* (57). It promotes aggregation of *C. difficile* cells *in vitro* (57) and confers resistance to *Siphoviridae* and *Myoviridae* family phages (58), but is expressed by only ~5% of cells in culture due to a phase-variable RecV-controlled genetic switch located between its promoter and coding DNA sequence (59). In bulk population measurements by qRT-PCR, *cwpV* expression was higher in the Δ*bapR* strain than WT and the complement, particularly in the presence of LCA (**Figure 5E**). However, the fold-change in *cwpV* expression induced by LCA (~2.5-fold in WT) was the same for Δ*bapR* and the Δ*bapR*/*bapR* complementation strain (**Figure 5F**). These data suggest that BapR indirectly represses *cwpV*, since the LCA-induced upregulation of *cwpV* is not dependent on BapR. Given that LCA causes global changes in the *C. difficile* transcriptional landscape (**Figure S5**), other unknown factors likely mediate the LCA-induced expression of *cwpV*.

Our RNA-seq analyses also identified a second cluster of genes whose expression changed in a BapR-dependent manner: *cd0618-0616*. The differential expression of *cd0616* and *cd0617* hovered at the significance cutoff, and *cd0618* approached significance under both conditions (**Figure 5A**). *cd0618* encodes a LytTR family transcription factor; *cd0617* encodes a CPBP family intramembrane metalloprotease; and *cd0616* encodes another MerR family transcription factor. TSSs were previously predicted for *cd0616* and *cd0618*, but not for *cd0617* (56) (**Figure 5B**). qRT-PCR analyses confirmed that these genes are over-expressed in the

Δ*bapR* strain relative to WT and the complement strain (**Figure 5G**), but only the expression of *cd0616* and *cd0617* was affected by LCA treatment (~2-fold reduction) (**Figure 5H**). LCA had similar effects on the expression of these genes between strains irrespective of whether BapR was present, indicating that like *cwpV,* BapR does not control their LCA-dependent expression (**Figure 5H**). While it is unclear whether there are other conditions in which BapR derepresses the expression of *cwpV* or the *cd0618-cd0616* locus, our data nonetheless imply that (i) BapR represses gene expression directly and indirectly and that (ii) separate, unknown mechanisms of LCA-dependent transcriptional regulation act in parallel to BapR.

BapR binds the promoter region of *mdeA* but not *cd0616*

To test whether BapR directly regulates the *mdeA* cluster, *cd0618* cluster, or *cwpV*, we performed electrophoretic mobility shift assays (EMSAs) with the promoter regions of these genes. These DNA fragments were fluorescently labeled at their 5' ends and incubated with purified BapR. Dose-dependent mobility shifts of the *mdeA* promoter region were observed for BapR, and importantly, this shift was competed away by an excess of the same promoter region lacking the fluorescent label (cold competitor; **Figure 6A**). In line with our transcriptional analyses suggesting that BapR indirectly regulates *cwpV*, no shift was seen for the *cwpV* promoter in its "on" orientation (**Figure 6B**) Further, BapR did not bind the promoters of *cd0618* or *cd0616* (**Figure S6**). BapR failed to bind its own promoter region indicating that it does not autoregulate (**Figure S6**).

Notably, we found that LCA addition to the EMSAs did not affect BapR binding to the *mdeA* promoter (**Figure 6A**). This result was not necessarily surprising given that MerR family transcription factors remain bound to their DNA targets regardless of whether their C-terminal domain has bound their ligands. Instead, ligand binding results in these transcription factors regulating transcription via DNA distortion to reorient the -35 and -10 sites and facilitate productive RNA polymerase interactions (51, 60, 61). Since MerR family proteins can act as repressors in

the absence of ligand and activators in the presence of ligand, our finding that BapR binds the *mdeA* promoter independently of LCA (**Figure 6A**) is consistent with previously characterized members of this family (60, 62–64). Furthermore, since BapR maintains the ability to bind DNA even in the presence of a large molar excess of LCA (**Figure 6A**), the reduced thermal stability of BapR observed in the presence of LCA (**Figure 2D**) is consistent with BapR undergoing a conformational change, rather than being destabilized by LCA.

Discussion

In this study, we identified BapR as a novel sensor for bile acids in *C. difficile* that de-represses the expression of a small subset of genes upon sensing LCA-related bile acids. Our chemical proteomics, affinity pull-downs, and thermal shift assays indicate that BapR specifically binds bile acids, especially LCA (**Figure 2**). Our data further suggest that BapR is stabilized by bile acids in *C. difficile* (**Figure 4**), which allows in BapR to directly de-repress the expression of genes encoding the methionine γ-lysase MdeA and two putative transporters. Specifically, our data indicate that BapR binds the promoter region of *mdeA* and represses the expression of the *mdeA* gene cluster in the absence of LCA; however, upon binding LCA, BapR undergoes a conformational change that reorients the *mdeA* promoter and licenses transcription (**Figure 7**). Given MdeA's involvement in sulfur metabolism (55) and the fact that bile acids are found exclusively in the gut of metazoans, we hypothesize that this LCA-sensing system regulates *C. difficile*'s metabolic adaptation to the gut environment. Since cysteine is elevated ~6-fold in the dysbiotic murine cecum (5), it is plausible that *C. difficile* would upregulate cysteine catabolism in this environment. Other factors downstream of this metabolic adaptation may be responsible for the cell length phenotype (**Figure 3**), but further studies are needed to delineate connections between these observations. Our RNA-Seq and qRT-PCR analyses also revealed that the expression of genes encoding the cell surface protein, CwpV, two other transcription factors, and

a putative metalloprotease is repressed by BapR (**Figures 5 and 6**), but conditions under which BapR may de-repress these genes remain to be determined.

Although BapR does not appear to be involved in resistance to LCA in the broth culture-based growth conditions tested, it is possible that the fitness of the Δ*bapR* strain would be reduced in competition with WT *in vitro* or *in vivo*. It is also possible that *C. difficile* has factors redundant to BapR that compensate for its loss. However, the strong correlation between presence of DCA and LCA in the gut and resistance to CDI could indicate that *C. difficile* does not have effective resistance mechanisms for these microbiota-generated metabolites. Instead, *C. difficile* appears to grow opportunistically in gut environments with very low levels of DCA and LCA (4–7), where these low levels could serve as environmental cues. Another possibility is that other stressors in the gut milieu could potentiate LCA's toxicity and reveal a resistance role for BapR. For example, antibiotics produced by 7α-dehydroxylating bacteria like *C. scindens*, which secretes 1-acetyl-β-carboline, and *Paraclostridium sordellii*, which produces turbomycin A and 1,1,1-tris(3-indolyl)-methane (TIM), are all active against *C. difficile* (36) and could potentiate the toxicity of LCA. While we attempted to test this hypothesis using the commercially available 1-acetyl-β-carboline, we unfortunately found that *C. difficile* strain 630Δ*erm* is substantially more resistant than the ATCC 9689 strain used in the study described above (36) (such that solubility limited our ability to test our hypothesis). Regardless, investigating the interactions between LCA-producing bacteria and *C. difficile* could reveal that LCA sensing by BapR gives rise to adaptations that confer a competitive advantage for *C. difficile*.

Determining the functions of the other genes repressed by BapR in an LCA-dependent manner may provide further insight into the function of this MerR family member. Notably, most MerR family transcription factors sense toxic molecules and upregulate cognate efflux pumps accordingly. Since *cd3575* is annotated as a sodium:solute symporter and *cd3576* a MFS transporter, a plausible function of this system is to transport metabolites related to cysteine catabolism. However, most bile acid-binding transcription factors in bacteria regulate production

of multidrug efflux pumps (65–68), and CD3575 and CD3576 could play a role in bile acid efflux. To date a transporter or channel for bile acids has not been identified in *C. difficile*, but we can infer this phenomenon from our chemical proteomics screen as the probes were added to intact cells in culture, washed away, then UV crosslinked. Indeed, many of the hits from our screen are cytosolic proteins (**Table S1**). A few examples of bacterial bile acid transporters have been described: the *baiG* gene found in 7α-dehydroxylating *Clostridium* and *Eubacterium* species encodes a bile acid transporter (29, 69), *Lactobacillus johnsonii* possesses a bile acid MFS transporter in conjunction with bile salt hydrolase activity (70), and *Neisseria meningitidis* and *Yersinia frederiksenii* both have a homologue of the eukaryotic ASBT sodium:bile acid co-transporter that imports TCA (71–74). *C. difficile* CD3575 and CD3576 share only 11-14% identity with each of these bile acid transporters, but the possibility remains that they export bile acids.

Only a few other bacterial transcription factors have been shown to directly sense bile acids (65–68), and to our knowledge BapR is the only example that detects bile acids for metabolic adaptation. While our data are consistent with BapR being a bile acid sensor, *C. difficile* almost certainly encodes alternative mechanisms for sensing or responding to LCA. Global transcriptional changes occur in the presence of LCA (**Figure S5**), yet BapR regulates the expression of only a handful of genes (**Figure 5**). Indeed, our chemical proteomics screen detected a few other putative transcription factors, two-component system histidine kinases, and serine/threonine kinases as candidate bile acid-binding proteins with potential signaling roles. Future studies of these hits could reveal pathways by which *C. difficile* deals with bile acid stress independent of BapR. For example, while we did not biochemically validate essential hits from our proteomics screen, inactivation of these proteins by LCA could explain its toxicity. Thus, it remains to be seen which are involved and whether the toxicity is due to the concerted inactivation of multiple proteins. Additional studies using bile acid photoaffinity probes and chemical proteomics should reveal other protein targets and mechanisms of action for these prominent gut microbiota metabolites.

Materials and Methods

Bacterial strains and growth conditions.

C. difficile strains are of the 630Δ*erm* background and mutants were constructed using *pyrE*-based allele-coupled exchange (54). Strains were grown on brain heart infusion medium supplemented with 0.5% w/v yeast extract and 0.1% w/v L-cysteine (BHIS) with taurocholate (TCA; 0.1% w/v; 1.9 mM), thiamphenicol (10–15 µg/mL), kanamycin (50 µg/mL), or cefoxitin (8 µg/mL) as needed. *C. difficile* defined medium (CDDM) (77)was supplemented with 5-fluoroorotic acid at 2 mg/mL and uracil at 5 µg/mL. Cultures were grown swirling at 37°C under anaerobic conditions using a gas mixture containing 85% N_2, 5% CO_2 and 10% H_2. *Escherichia coli* strains were grown at 37°C with shaking at 225 rpm in Luria-Bertani medium (LB) or at 20˚C with shaking at 225 rpm in autoinduction broth (Terrific broth [Thermo Fisher] with 0.5% glycerol, 0.05% glucose, and 0.1% α-lactose monohydrate). Media were supplemented with chloramphenicol (20 µg/mL), ampicillin (100 µg/mL), or kanamycin (30 µg/mL) as needed.

C. difficile growth curves.

C. difficile cultures were grown for 3 hours, back-diluted 1:50, and grown for an additional 3 hours to an OD_{600} of ~0.3. Cultures were diluted to an OD_{600} of 0.05 and added to 96-well plates with 2X pre-reduced bile acids or probes in BHIS for a total volume of 150 µL/well (75 µL culture + 75 µL 2X compound in BHIS). OD_{600} was read every 10 minutes for 18 hours with constant shaking at 37˚C in an Epoch 2 plate reader (BioTek) in an anaerobic chamber. Percent growth inhibition was calculated from the OD_{600} relative to DMSO at 5 hours. Two biological replicates from independent starter cultures were used per experiment.

In-gel fluorescent bile acid probe labeling.

C. difficile cultures were grown for 3 hours, back-diluted 1:25 into 25 mL BHIS, and grown for an additional 3-4 hours to an OD_{600} of ~0.7. Bile acid probes or DMSO were added to the cultures and incubated for 30 minutes. Cells were resuspended in 1 mL PBS, transferred to a 24-well plate, and UV irradiated (365 nm) uncovered for 5 minutes on ice 3-5 cm from the lamp. Probe-crosslinked cells were pelleted, resuspended in 500 µL cold lysis buffer (1X Halt protease inhibitor [Thermo Fisher], 0.5 mg/mL lysozyme, 1:1000 benzonase [EMD Millipore], and 0.1% NP-40 in 1X PBS). Cells were lysed by four 30-second rounds of bead beating at speed 6 with Lysing Matrix B (MP Bio) in a Fast Prep-24 bead beater (MP Bio). Beads were pelleted at 3,000g for 2 minutes and the total lysate was collected. Alexa Fluor 488 was conjugated to the probe in 30 µg total lysate using a Click-iT Plus Alexa Fluor 488 Picolyl Azide Toolkit (Thermo Fisher). Protein was precipitated overnight at -20˚C in methanol, washed twice with cold methanol, and resuspended in 25 µL SDS-PAGE sample buffer. Fluorescent probe labeling was visualized in-gel following SDS-PAGE using the SYBR Safe long pass blue filter in a Fujifilm FLA-9000 imager at 200 µM resolution. The gel was Coomassie stained as a loading control.

Chemical proteomics.

C. difficile overnight cultures were diluted 1:25 into 20 mL BHIS and grown to an OD_{600} of 1.1. Bile acid probes or DMSO were added at 10 µM for 1 hour. Cells were resuspended in 1 mL phosphate-buffered solution (PBS), transferred to a 24-well plate, and UV irradiated (365 nm) uncovered for 5 minutes on ice 3-5 cm from the lamp. Probe-crosslinked cells were pelleted, resuspended in 500 µL cold lysis buffer (1X Halt protease inhibitor [Thermo Fisher], 0.5 mg/mL lysozyme, 1:1000 benzonase [EMD Millipore], and 0.1% NP-40 in 1X PBS). Cells were lysed by four 30-second rounds of bead beating at speed 6 with Lysing Matrix B (MP Bio) in a Fast Prep-24 bead beater (MP Bio). Beads were pelleted at 3,000 g for 2 minutes and the total lysate was collected. The lysate was flash-frozen in liquid nitrogen before further processing. Cell lysates were centrifuged at 16000 g for 20 min to remove cell debris and supernatants were collected.

Each total cell lysates was added with 100 µL of click chemistry reagents as a 10X master mix (az-Biotin: 0.1 mM, 10 mM stock solution in DMSO; tris(2-carboxyethyl)phosphine hydrochloride (TCEP): 1 mM, 50 mM freshly prepared stock solution in dH_2O; tris[(1-benzyl-1H-1,2,3-triazol-4-yl)methyl]amine (TBTA): (0.1 mM, 2 mM stock in 4:1 *t*-butanol: DMSO); $CuSO_4$ (1 mM, 50 mM freshly prepared stock in dH_2O). Samples were mixed well and incubated at room temperature for 1 h. After incubation, samples were mixed with 4 mL cold methanol and incubated at -20 °C overnight. Protein pellets were centrifuged at 5000 g for 30 min at 4°C, pellets were transferred to 2.0 mL centrifuge tube and were washed with 1 mL cold methanol 3 times. After last wash, pellets were let air dried before being re-solubilized in 250 µL 4% SDS PBS with bath sonication. Solutions were diluted with 750 µL PBS, and incubated with 100 µL PBS-T-washed High Capacity NeutrAvidin agarose (Pierce) (500 µL PBS-T-washed twice, 2500 g for 60 s) at room temperature for 1 h with end-to-end rotation. The agarose was washed with 500 µL 1% SDS PBS 3 times, 500 µL 1M Urea PBS 3 times, and 500 µL PBS, 3 times and then reduced with 500 µL 10 mM DTT (Sigma) in PBS for 30 min at 37 °C, and alkylated with 500 µL 50 mM iodoacetamide (Sigma) in PBS for 30 min in dark. 50 µL NH_4HCO_3 (10 mM) was added to the tube. Neutravidin-bound proteins were digested on bead with 400 ng Trypsin/Lys-C mix (Promega) at 37 °C overnight with shaking. Digested peptides were collected (2500 g for 60 s) and lyophilized before being desalted with custom-made stage-tip containing Empore SPE Extraction Disk (3M). Peptides were eluted with 2% acetonitrile, 2% formic acid in dH_2O.

Peptide LC-MS analysis was performed with a Dionex 3000 nano-HPLC coupled to an Orbitrap XL mass spectrometer (Thermo Fisher). Peptide samples were pressure-loaded onto a home-made C18 reverse-phase column (75 µm diameter, 15 cm length). A 180-minute gradient increasing from 95% buffer A (HPLC grade water with 0.1% formic acid) and 5% buffer B (HPLC grade acetonitrile with 0.1% formic acid) to 75% buffer B in 133 minutes was used at 200 nL/min. The Orbitrap XL was operated in top-8-CID-mode with MS spectra measured at a resolution of

60,000@m/z 400. One full MS scan (300–2000 MW) was followed by three data-dependent scans of the most intense ions with dynamic exclusion enabled. Label-free quantification of bile acid probe-labeled proteins was performed in MaxQuant software as described (78). The search results from MaxQuant were analyzed by Perseus (http://www.perseusframework.org/). Briefly, the DMSO and bile acid probe-labeled replicates were grouped correspondingly. The results were cleaned to filter off reverse hits and contaminants. Only proteins that were identified in 3 out of 4 sample replicates and with more than two unique peptides were subjected to subsequent statistical analysis. LFQ intensities were used for measuring protein abundance and logarithmized (base 2). Signals that were originally zero were imputed with random numbers from a normal distribution, whose mean and standard deviation were chosen to best simulate low abundance values below the noise level (Normal distribution: Width = 0.3; Shift = 1.8).

Bile acid probe pull-downs of BapR.

C. difficile cultures were grown for 4 hours, back-diluted 1:2,000 into 70 mL BHIS, and grown overnight. Cultures were then diluted to an OD_{600} of 1, split into 20 mL/condition and incubated with probe or DMSO for 1 hour. Cells were resuspended in 1 mL PBS, transferred to a 6-well plate, and UV irradiated (365 nm) uncovered for 5 minutes on ice 3-5 cm from the lamp. Probe-crosslinked cells were pelleted, resuspended in 1 mL cold lysis buffer (1X Halt protease inhibitor [Thermo Fisher], 0.5 mg/mL lysozyme, 1:1000 benzonase [EMD Millipore], and 0.1% NP-40 in 1X PBS). Cells were lysed by four 30-second rounds of bead beating at speed 6 with Lysing Matrix B (MP Bio) in a Fast Prep-24 bead beater (MP Bio). Beads were pelleted at 21,000g for 5 minutes at 4˚C and the cleared lysate was collected. Biotin was conjugated to the probes in a click reaction with 0.4 mg cleared lysate in 180 µL PBS and 20 µL 10X click master mix (1 mM azido-PEG3-biotin [Alfa Aesar], 10 mM tris(2-carboxyethyl)phosphine hydrochloride, 1 mM tris[(1-benzyl-1H-1,2,3-triazol-4-yl)methyl]amine in 4:1 t-butanol:DMSO, and 10 mM copper sulfate pentahydrate) and protein was precipitated overnight at -20˚C in methanol. Precipitates were

526 washed twice with cold methanol, dried at 37˚C for 1 hour, and resolubilized in 50 µL 4% sodium
527 dodecyl sulfate (SDS) in PBS with bath sonication. 150 µL PBS was added and a sample was
528 taken as input before incubation with PBS+0.1% Tween-20-washed Pierce High Capacity
529 NeutrAvidin agarose beads (Thermo Fisher) for 1 hour at room temperature with end-over-end
530 rotation. Beads were washed three times each with PBS+1% SDS, PBS+4M urea, then PBS and
531 boiled to elute biotin-probe-protein complexes.
532
533 **Recombinant BapR purification.**
534 BL21(DE3) *E. coli* encoding lactose-inducible *bapR* with a C-terminal autoprocessing CPD-His
535 tag was grown in 20 mL LB with ampicillin, then back-diluted 1:1,000 into 1L autoinduction broth
536 with ampicillin and grown at 20˚C for ~60 hours. Cultures were pelleted, resuspended in 50 mL
537 low imidazole buffer (LIB; 500 mM NaCl, 50 mM Tris-HCl pH 7.5, 15 mM imidazole, 10% glycerol,
538 2 mM β-mercaptoethanol), and flash frozen in liquid nitrogen. Once thawed, cells were probe
539 sonicated (Branson) in 3 x 45 second rounds at 40% amplitude with 5 minutes on ice between.
540 Lysates were cleared by centrifugation at 13,000 rpm for 45 min at 4˚C. BapR-CPD-His was
541 affinity purified from cleared lysates using Ni-NTA agarose beads (Qiagen) with gentle rocking at
542 4˚C for 2 hours. The beads were washed three times with LIB before inducing cleavage of the
543 CPD tag (79) with 200 µM inositol hexakisphosphate in LIB at 4˚C overnight to elute untagged
544 BapR. The eluted protein was buffer-exchanged into SEC buffer (200 mM NaCl, 10 mM Tris-HCl
545 pH 7.5, 5% glycerol, and 1 mM dithiothreitol) and concentrated using an Amicon Ultra-15 10 kDa
546 cutoff centrifugal filter (Millipore Sigma). Affinity-purifued protein was further purified by size
547 exclusion chromatography (SEC) using a Superdex 200 Increase 10/300 GL column (GE) on an
548 AKTA Pure fast protein liquid chromatography instrument (GE), reconcentrated, and flash frozen
549 in aliquots.
550
551 **Thermal shift assays.**

552 Affinity- and SEC-purified BapR was added to a mix of 5X SYPRO Orange dye (Thermo Fisher)
553 and the indicated concentrations of bile acids or DMSO in 1.5X PBS to a final concentration of 1
554 μM in a 96-well white bottom plate. Fluorescence was measured as temperature increased
555 1˚C/minute from 25˚C to 95˚C in a StepOne Plus qPCR instrument (Applied Biosystems). Protein
556 from 2 independent purifications was used, and a no-protein control for each ligand at each
557 concentration was used to identify cutoffs above which the ligand generated background
558 fluorescence, if at all.
559
560 **Phase-contrast microscopy.**
561 *C. difficile* was inoculated into BHIS cultures and grown for 3 hours, back-diluted 1:50, and grown
562 for another 3 hours. Cultures were then split and treated with DMSO or bile acids at the indicated
563 concentrations for 3 hours. Aliquots of the cultures were pelleted, resuspended in ~20 μL PBS,
564 and 1 μL was spotted on a 1% agarose pad poured in a Gene Frame (Thermo Fisher). Pads were
565 sealed with a coverslip inside the anaerobic chamber. Phase images were acquired on a Zeiss
566 Axioskop using a 100X Plan-NEOFLUAR oil phase objective. Cell length was measured from
567 pole-to-pole using Fiji software and at least 460 cells were measured per strain/condition in 5
568 independent experiments.
569
570 **BapR protein induction by bile acids in *C. difficile*.**
571 *C. difficile* starter cultures were grown for 3 hours, back-diluted 1:50 into 30 mL BHIS, and grown
572 for an additional 3 hours before being split into new tubes with the indicated concentrations of bile
573 acids or DMSO. After 3 hours cells were pelleted, resuspended in sample loading buffer, frozen
574 at -20C, and boiled before running SDS-PAGE. Protein was transferred to a PVDF membrane,
575 blocked with 0.5X blocking buffer (LI-COR), and probed with chicken α-GDH antibody (Thermo
576 Fisher) and a custom mouse α-BapR antibody (Cocalico Biologicals). Antibodies were detected
577 using IRDye700- or IRDye800-conjugated donkey α-chicken and goat α-mouse secondary

antibodies (LI-COR). The blots were imaged using a LI-COR Odyssey CLx imager and quantified using ImageStudio Lite software (LI-COR).

RNA extraction, RNA-seq, and qRT-PCR.

C. difficile cultures were grown for 3-4 hours, back-diluted 1:50, and grown for an additional 3-4 hours before being split for treatment with DMSO or 20 μM LCA. After 1 or 3 hours of LCA exposure (OD_{600} of 0.1-0.2 at 1 hour or 0.2-0.5 at 3 hours) RNA was extracted using a FastRNA Pro Blue kit (MP Bio). Samples were treated twice for 45 minutes at 37˚C with DNase I (New England Biolabs) with heat inactivation at 75˚C for 10 minutes and DNA was further removed using a RNeasy Mini kit (Qiagen). RNA was harvested from three independent cultures as biological replicates per experiment, and independent extractions were used for RNA-seq and qRT-PCR validation.

For RNA-seq analysis an Agilent Bioanalyzer was used to verify RNA quality before depleting rRNA and ligating adapters and indexes using a Stranded Total RNA with RiboZero Plus library preparation kit (Illumina). Samples were sequenced as single-end 75 reads on an Illumina NextSeq 500 sequencer at the Tufts University Genomics Core Facility. Sequences were trimmed using BBDuk, mapped to the *C. difficile* 630 genome, and analyzed for differential expression using DESeq2 in Geneious Prime software. Gene functional characterization was done using GSEA-Pro v3 (University of Groningen) to classify by COG terms and manual classification for genes that were not classified by GSEA-Pro.

For qRT-PCR analysis an Ambion Microbe Express kit (Invitrogen) was used to enrich mRNA. cDNA was synthesized using a SuperScript First Strand Synthesis kit (Invitrogen). qPCR was performed using Luna Universal qPCR Master Mix (New England Biolabs) with 1:5 diluted cDNA in technical duplicate in a StepOne Plus qPCR instrument (Applied Biosystems). A standard curve made from plasmid encoding the gene of interest or a purified PCR product was used to enumerate gene copies in each sample. A no-RT control sample was used to ensure no

DNA contamination. Primers were designed using the Integrated DNA Technologies Primer Quest tool.

Electrophoretic mobility shift assays (EMSAs).

Unlabeled DNA fragments (200-250 bp) encompassing putative promoter regions were amplified from purified *C. difficile* 630Δ*erm* genomic DNA, purified with a GeneJet gel extraction kit (Thermo Fisher), and used as cold competitors or as templates for PCR with IRDye800-conjugated primers (Integrated DNA Technologies). The labeled DNA fragments were purified with a GeneJet PCR purification kit (Thermo Fisher). 20 fmol labeled DNA (or 20 fmol labeled with 1,000 fmol unlabeled for cold competitor control) was mixed with purified BapR and DMSO or 1 μM LCA in binding buffer (20 mM Tris-HCl pH 8, 10 mM KCl, 2 mM $MgCl_2$, 0.5 mM EDTA, 1 mM DTT, 0.05% Nonidet-P40, 12% v/v glycerol, 25 μg/mL salmon sperm DNA) for 20 minutes at room temperature and run on a 8% native polyacrylamide gel at 225V at 4˚C in the dark. DNA was visualized using an Odyssey CLx imager (LI-COR).

Data visualization and statistics.

All graphs were generated using Prism 9 software (GraphPad). Chemical structures were generated using ChemDraw 20.0 software (Perkin Elmer). Statistical analyses were done using Prism 9 software (GraphPad).

References

1. Abt MC, McKenney PT, Pamer EG. 2016. *Clostridium difficile* colitis: pathogenesis and host defence. Nat Rev Microbiol 14:609–620.

2. Rupnik M, Wilcox MH, Gerding DN. 2009. *Clostridium difficile* infection: new developments in epidemiology and pathogenesis. 7. Nat Rev Microbiol 7:526–536.

3. Guh AY, Mu Y, Winston LG, Johnston H, Olson D, Farley MM, Wilson LE, Holzbauer SM, Phipps EC, Dumyati GK, Beldavs ZG, Kainer MA, Karlsson M, Gerding DN, McDonald LC. 2020. Trends in U.S. Burden of *Clostridioides difficile* Infection and Outcomes. New Engl J Med.

4. Koenigsknecht MJ, Theriot CM, Bergin IL, Schumacher CA, Schloss PD, Young VB. 2015. Dynamics and establishment of *Clostridium difficile* infection in the murine gastrointestinal tract. Infect Immun 83:934–941.

5. Theriot CM, Koenigsknecht MJ, Carlson PE, Hatton GE, Nelson AM, Li B, Huffnagle GB, Z Li J, Young VB. 2014. Antibiotic-induced shifts in the mouse gut microbiome and metabolome increase susceptibility to *Clostridium difficile* infection. Nat Commun 5:3114.

6. Theriot CM, Bowman AA, Young VB. 2016. Antibiotic-Induced Alterations of the Gut Microbiota Alter Secondary Bile Acid Production and Allow for *Clostridium difficile* Spore Germination and Outgrowth in the Large Intestine. mSphere 1.

7. Buffie CG, Bucci V, Stein RR, McKenney PT, Ling L, Gobourne A, No D, Liu H, Kinnebrew M, Viale A, Littmann E, van den Brink MRM, Jenq RR, Taur Y, Sander C, Cross JR, Toussaint NC, Xavier JB, Pamer EG. 2015. Precision microbiome reconstitution restores bile acid mediated resistance to Clostridium difficile. Nature 517:205–208.

8. Weingarden AR, Chen C, Bobr A, Yao D, Lu Y, Nelson VM, Sadowsky MJ, Khoruts A. 2014. Microbiota transplantation restores normal fecal bile acid composition in recurrent *Clostridium difficile* infection. Am J Physiol Gastrointest Liver Physiol 306:G310–G319.

9. Sato Y, Atarashi K, Plichta DR, Arai Y, Sasajima S, Kearney SM, Suda W, Takeshita K, Sasaki T, Okamoto S, Skelly AN, Okamura Y, Vlamakis H, Li Y, Tanoue T, Takei H, Nittono H, Narushima S, Irie J, Itoh H, Moriya K, Sugiura Y, Suematsu M, Moritoki N, Shibata S, Littman DR, Fischbach MA, Uwamino Y, Inoue T, Honda A, Hattori M, Murai T, Xavier RJ, Hirose N, Honda K. 2021. Novel bile acid biosynthetic pathways are enriched in the microbiome of centenarians. Nature 599:458–464.

10. Ridlon JM, Kang D-J, Hylemon PB. 2006. Bile salt biotransformations by human intestinal bacteria. J Lipid Res 47:241–259.

11. Hamilton JP, Xie G, Raufman J-P, Hogan S, Griffin TL, Packard CA, Chatfield DA, Hagey LR, Steinbach JH, Hofmann AF. 2007. Human cecal bile acids: concentration and spectrum. Amer J Physiol Gastrointest Liver Physiol 293:G256–G263.

12. Yoshimoto S, Loo TM, Atarashi K, Kanda H, Sato S, Oyadomari S, Iwakura Y, Oshima K, Morita H, Hattori M, Hattori M, Honda K, Ishikawa Y, Hara E, Ohtani N. 2013. Obesity-induced gut microbial metabolite promotes liver cancer through senescence secretome. Nature 499:97–101.

13. Winston JA, Rivera AJ, Cai J, Thanissery R, Montgomery SA, Patterson AD, Theriot CM. 2020. Ursodeoxycholic Acid (UDCA) Mitigates the Host Inflammatory Response during Clostridioides difficile Infection by Altering Gut Bile Acids. Infect Immun 88:e00045-20.

14. Ma C, Han M, Heinrich B, Fu Q, Zhang Q, Sandhu M, Agdashian D, Terabe M, Berzofsky JA, Fako V, Ritz T, Longerich T, Theriot CM, McCulloch JA, Roy S, Yuan W, Thovarai V,

Sen SK, Ruchirawat M, Korangy F, Wang XW, Trinchieri G, Greten TF. 2018. Gut microbiome-mediated bile acid metabolism regulates liver cancer via NKT cells. Science 360:eaan5931.

15. Song X, Sun X, Oh SF, Wu M, Zhang Y, Zheng W, Geva-Zatorsky N, Jupp R, Mathis D, Benoist C, Kasper DL. 2020. Microbial bile acid metabolites modulate gut RORγ+ regulatory T cell homeostasis. Nature 577:410–415.

16. Winkler ES, Shrihari S, Hykes BL, Handley SA, Andhey PS, Huang Y-JS, Swain A, Droit L, Chebrolu KK, Mack M, Vanlandingham DL, Thackray LB, Cella M, Colonna M, Artyomov MN, Stappenbeck TS, Diamond MS. 2020. The intestinal microbiome restricts alphavirus infection and dissemination through a bile acid-type I IFN signaling axis. Cell 182:901-918.e18.

17. Campbell C, McKenney PT, Konstantinovsky D, Isaeva OI, Schizas M, Verter J, Mai C, Jin W-B, Guo C-J, Violante S, Ramos RJ, Cross JR, Kadaveru K, Hambor J, Rudensky AY. 2020. Bacterial metabolism of bile acids promotes generation of peripheral regulatory T cells. 7809. Nature 581:475–479.

18. Li W, Hang S, Fang Y, Bae S, Zhang Y, Zhang M, Wang G, McCurry MD, Bae M, Paik D, Franzosa EA, Rastinejad F, Huttenhower C, Yao L, Devlin AS, Huh JR. 2021. A bacterial bile acid metabolite modulates Treg activity through the nuclear hormone receptor NR4A1. Cell Host & Microbe 29:1366-1377.e9.

19. Paik D, Yao L, Zhang Y, Bae S, D'Agostino GD, Zhang M, Kim E, Franzosa EA, Avila-Pacheco J, Bisanz JE, Rakowski CK, Vlamakis H, Xavier RJ, Turnbaugh PJ, Longman RS, Krout MR, Clish CB, Rastinejad F, Huttenhower C, Huh JR, Devlin AS. 2022. Human gut bacteria produce TH17-modulating bile acid metabolites. Nature 1–6.

20. Sinha SR, Haileselassie Y, Nguyen LP, Tropini C, Wang M, Becker LS, Sim D, Jarr K, Spear ET, Singh G, Namkoong H, Bittinger K, Fischbach MA, Sonnenburg JL, Habtezion A. 2020. Dysbiosis-Induced Secondary Bile Acid Deficiency Promotes Intestinal Inflammation. Cell Host & Microbe 2020.

21. Grau KR, Zhu S, Peterson ST, Helm EW, Philip D, Phillips M, Hernandez A, Turula H, Frasse P, Graziano VR, Wilen CB, Wobus CE, Baldridge MT, Karst SM. 2020. Commensal bacteria regulate regionalization of acute norovirus infection along the intestinal tract through bile acid-mediated priming of type III interferon. Nat Microbiol 5:84–92.

22. Vidal JE, Wier MN, A Angulo-Zamudio U, McDevitt E, Jop Vidal AG, Alibayov B, Scasny A, Wong SM, Akerley BJ, McDaniel LS. 2021. Prophylactic Inhibition of Colonization by *Streptococcus pneumoniae* with the Secondary Bile Acid Metabolite Deoxycholic Acid. Infect Immun 89:e0046321.

23. Urdaneta V, Casadesús J. 2017. Interactions between Bacteria and Bile Salts in the Gastrointestinal and Hepatobiliary Tracts. Front Med (Lausanne) 4:163.

24. Ruiz L, Margolles A, Sánchez B. 2013. Bile resistance mechanisms in *Lactobacillus* and *Bifidobacterium*. Front Microbiol 4:396.

25. Ridlon JM, Kang D-J, Hylemon PB. 2010. Isolation and Characterization of a Bile Acid Inducible 7α-dehydroxylating operon in *Clostridium hylemonae* TN271. Anaerobe 16:137–146.

26. Kang D-J, Ridlon JM, Moore DR, Barnes S, Hylemon PB. 2008. *Clostridium scindens baiCD* and *baiH* genes encode stereo-specific 7α/7β-hydroxy-3-oxo-Δ4-cholenoic acid oxidoreductases. Biochim Biophys Acta 1781:16–25.

715 27. Dawson JA, Mallonee DH, Björkhem I, Hylemon PB. 1996. Expression and
716 characterization of a C24 bile acid 7 alpha-dehydratase from *Eubacterium* sp. strain VPI
717 12708 in Escherichia coli. Journal of Lipid Research 37:1258–1267.

718 28. Mallonee DH, White WB, Hylemon PB. 1990. Cloning and sequencing of a bile acid-
719 inducible operon from *Eubacterium* sp. strain VPI 12708. J Bacteriol 172:7011–7019.

720 29. Wells JE, Hylemon PB. 2000. Identification and Characterization of a Bile Acid 7α-
721 Dehydroxylation Operon in *Clostridium* sp. Strain TO-931, a Highly Active 7α-
722 Dehydroxylating Strain Isolated from Human Feces. Appl Environ Microbiol 66:1107–1113.

723 30. Solbach P, Chhatwal P, Woltemate S, Tacconelli E, Buhl M, Gerhard M, Thoeringer CK,
724 Vehreschild MJGT, Jazmati N, Rupp J, Manns MP, Bachmann O, Suerbaum S. 2018.
725 *BaiCD* gene cluster abundance is negatively correlated with *Clostridium difficile* infection.
726 PLOS ONE 13:e0196977.

727 31. Reed AD, Nethery MA, Stewart A, Barrangou R, Theriot CM. 2020. Strain-Dependent
728 Inhibition of *Clostridioides difficile* by Commensal Clostridia Carrying the Bile Acid-
729 Inducible (*bai*) Operon. J Bacteriol 202:e00039-20.

730 32. Aguirre AM, Yalcinkaya N, Wu Q, Swennes A, Tessier ME, Roberts P, Miyajima F,
731 Savidge T, Sorg JA. 2021. Bile acid-independent protection against *Clostridioides difficile*
732 infection. PLoS Pathog 17:e1010015.

733 33. Studer N, Desharnais L, Beutler M, Brugiroux S, Terrazos MA, Menin L, Schürch CM,
734 McCoy KD, Kuehne SA, Minton NP, Stecher B, Bernier-Latmani R, Hapfelmeier S. 2016.
735 Functional Intestinal Bile Acid 7α-Dehydroxylation by Clostridium scindens Associated with
736 Protection from *Clostridium difficile* Infection in a Gnotobiotic Mouse Model. Frontiers in
737 Cellular and Infection Microbiology 6:191.

738 34. Weingarden AR, Dosa PI, DeWinter E, Steer CJ, Shaughnessy MK, Johnson JR, Khoruts
739 A, Sadowsky MJ. 2016. Changes in Colonic Bile Acid Composition following Fecal
740 Microbiota Transplantation Are Sufficient to Control *Clostridium difficile* Germination and
741 Growth. PLoS One 11.

742 35. Lewis BB, Carter RA, Pamer EG. 2016. Bile acid sensitivity and in vivo virulence of clinical
743 *Clostridium difficile* isolates. Anaerobe 41:32–36.

744 36. Kang JD, Myers CJ, Harris SC, Kakiyama G, Lee I-K, Yun B-S, Matsuzaki K, Furukawa M,
745 Min H-K, Bajaj JS, Zhou H, Hylemon PB. 2019. Bile Acid 7α-Dehydroxylating Gut Bacteria
746 Secrete Antibiotics that Inhibit *Clostridium difficile*: Role of Secondary Bile Acids. Cell
747 Chemical Biology 26:27-34.e4.

748 37. Sistrunk JR, Nickerson KP, Chanin RB, Rasko DA, Faherty CS. 2016. Survival of the
749 Fittest: How Bacterial Pathogens Utilize Bile To Enhance Infection. Clinical Microbiology
750 Reviews 29:819–836.

751 38. Sievers S, Metzendorf NG, Dittmann S, Troitzsch D, Gast V, Tröger SM, Wolff C, Zühlke
752 D, Hirschfeld C, Schlüter R, Riedel K. 2019. Differential View on the Bile Acid Stress
753 Response of *Clostridioides difficile*. Front Microbiol 10:258.

754 39. Dubois T, Tremblay YDN, Hamiot A, Martin-Verstraete I, Deschamps J, Monot M, Briandet
755 R, Dupuy B. 2019. A microbiota-generated bile salt induces biofilm formation in *Clostridium*
756 *difficile*. NPJ Biofilms Microbiomes 5.

757 40. Tam J, Icho S, Utama E, Orrell KE, Gómez-Biagi RF, Theriot CM, Kroh HK, Rutherford SA,
758 Lacy DB, Melnyk RA. 2020. Intestinal bile acids directly modulate the structure and
759 function of *C. difficile* TcdB toxin. Proc Natl Acad Sci USA 117:6792–6800.

760 41. Thanissery R, Winston JA, Theriot CM. 2017. Inhibition of spore germination, growth, and
761 toxin activity of clinically relevant *C. difficile* strains by gut microbiota derived secondary
762 bile acids. Anaerobe 45:86–100.

763 42. Francis MB, Allen CA, Shrestha R, Sorg JA. 2013. Bile Acid Recognition by the *Clostridium*
764 *difficile* Germinant Receptor, CspC, Is Important for Establishing Infection. PLoS
765 Pathogens 9:e1003356.

766 43. Sorg JA, Sonenshein AL. 2008. Bile salts and glycine as cogerminants for Clostridium
767 difficile spores. J Bacteriol 190:2505–12.

768 44. Parasar B, Zhou H, Xiao X, Shi Q, Brito IL, Chang PV. 2019. Chemoproteomic Profiling of
769 Gut Microbiota-Associated Bile Salt Hydrolase Activity. ACS Cent Sci 5:867–873.

770 45. Dembek M, Barquist L, Boinett CJ, Cain AK, Mayho M, Lawley TD, Fairweather NF, Fagan
771 RP. 2015. High-throughput analysis of gene essentiality and sporulation in *Clostridium*
772 *difficile*. mBio 6:e02383.

773 46. Schumacher MA, Brennan RG. 2002. Structural mechanisms of multidrug recognition and
774 regulation by bacterial multidrug transcription factors. Mol Microbiol 45:885–893.

775 47. Roy A, Kucukural A, Zhang Y. 2010. I-TASSER: a unified platform for automated protein
776 structure and function prediction. Nat Protoc 5:725–738.

777 48. Brown NL, Stoyanov JV, Kidd SP, Hobman JL. 2003. The MerR family of transcriptional
778 regulators. FEMS Microbiology Reviews 27:145–163.

779 49. Markham PN, Loguidice J, Neyfakh AA. 1997. Broad Ligand Specificity of the
780 Transcriptional Regulator of the *Bacillus subtilis* Multidrug Transporter Bmr. Biochem
781 Biophys Res Comm 239:269–272.

782 50. Vázquez-Laslop N, Markham PN, Neyfakh AA. 1999. Mechanism of Ligand Recognition by
783 BmrR, the Multidrug-Responding Transcriptional Regulator: Mutational Analysis of the
784 Ligand-Binding Site. Biochemistry 38:16925–16931.

785 51. Heldwein EEZ, Brennan RG. 2001. Crystal structure of the transcription activator BmrR
786 bound to DNA and a drug. 6818. Nature 409:378–382.

787 52. Hamiaux C, Drummond RSM, Janssen BJ, Ledger SE, Cooney JM, Newcomb RD,
788 Snowden KC. 2012. DAD2 Is an α/β Hydrolase Likely to Be Involved in the Perception of
789 the Plant Branching Hormone, Strigolactone. Curr Biol 22:2032–2036.

790 53. Kabir A, Honda RP, Kamatari YO, Endo S, Fukuoka M, Kuwata K. 2016. Effects of ligand
791 binding on the stability of aldo–keto reductases: Implications for stabilizer or destabilizer
792 chaperones. Prot Sci 25:2132–2141.

793 54. Ng YK, Ehsaan M, Philip S, Collery MM, Janoir C, Collignon A, Cartman ST, Minton NP.
794 2013. Expanding the Repertoire of Gene Tools for Precise Manipulation of the *Clostridium*
795 *difficile* Genome: Allelic Exchange Using *pyrE* Alleles. PLoS ONE 8.

796 55. Dubois T, Dancer-Thibonnier M, Monot M, Hamiot A, Bouillaut L, Soutourina O, Martin-
797 Verstraete I, Dupuy B. 2016. Control of *Clostridium difficile* Physiopathology in Response
798 to Cysteine Availability. Infect Immun 84:2389–2405.

799 56. Soutourina O, Dubois T, Monot M, Shelyakin PV, Saujet L, Boudry P, Gelfand MS, Dupuy
800 B, Martin-Verstraete I. 2020. Genome-Wide Transcription Start Site Mapping and Promoter
801 Assignments to a Sigma Factor in the Human Enteropathogen *Clostridioides difficile*. Front
802 Microbiol 11.

803 57. Reynolds CB, Emerson JE, de la Riva L, Fagan RP, Fairweather NF. 2011. The
804 *Clostridium difficile* Cell Wall Protein CwpV is Antigenically Variable between Strains, but
805 Exhibits Conserved Aggregation-Promoting Function. PLoS Pathog 7:e1002024.

806 58. Sekulovic O, Ospina Bedoya M, Fivian-Hughes AS, Fairweather NF, Fortier L. 2015. The
807 *Clostridium difficile* cell wall protein CwpV confers phase-variable phage resistance. Mol
808 Microbiol 98:329–342.

809 59. Emerson JE, Reynolds CB, Fagan RP, Shaw HA, Goulding D, Fairweather NF. 2009. A
810 novel genetic switch controls phase variable expression of CwpV, a *Clostridium difficile* cell
811 wall protein. Mol Microbiol 74:541–556.

812 60. Ansari AZ, Bradner JE, O'Halloran TV. 1995. DNA-bend modulation in a repressor-to-
813 activator switching mechanism. Nature 374:371–375.

814 61. Outten CE, Outten FW, O'Halloran TV. 1999. DNA distortion mechanism for transcriptional
815 activation by ZntR, a Zn(II)-responsive MerR homologue in Escherichia coli. J Biol Chem
816 274:37517–37524.

817 62. Philips SJ, Canalizo-Hernandez M, Yildirim I, Schatz GC, Mondragón A, O'Halloran TV.
818 2015. Allosteric Transcriptional Regulation via changes in the Overall Topology of the Core
819 Promoter. Science 349:877–881.

820 63. Shewchuk LM, Helmann JD, Ross W, Park SJ, Summers AO, Walsh CT. 1989.
821 Transcriptional switching by the MerR protein: activation and repression mutants implicate
822 distinct DNA and mercury(II) binding domains. Biochemistry 28:2340–2344.

64. Chang C-C, Lin L-Y, Zou X-W, Huang C-C, Chan N-L. 2015. Structural basis of the mercury(II)-mediated conformational switching of the dual-function transcriptional regulator MerR. Nucleic Acids Res 43:7612–7623.

65. Beggs GA, Zalucki YM, Brown NG, Rastegari S, Phillips RK, Palzkill T, Shafer WM, Kumaraswami M, Brennan RG. 2019. Structural, Biochemical, and In Vivo Characterization of MtrR-Mediated Resistance to Innate Antimicrobials by the Human Pathogen *Neisseria gonorrhoeae*. J Bacteriol 201.

66. Lei H-T, Shen Z, Surana P, Routh MD, Su C-C, Zhang Q, Yu EW. 2011. Crystal structures of CmeR-bile acid complexes from *Campylobacter jejuni*. Prot Sci 20:712–23.

67. Quillin SJ, Schwartz KT, Leber JH. 2011. The novel *Listeria monocytogenes* bile sensor BrtA controls expression of the cholic acid efflux pump MdrT. Mol Microbiol 81:129–142.

68. Nikaido E, Yamaguchi A, Nishino K. 2008. AcrAB multidrug efflux pump regulation in *Salmonella enterica* serovar Typhimurium by RamA in response to environmental signals. J Biol Chem 283:24245–24253.

69. Mallonee DH, Hylemon PB. 1996. Sequencing and expression of a gene encoding a bile acid transporter from *Eubacterium* sp. strain VPI 12708. J Bacteriol 178:7053–7058.

70. Elkins CA, Moser SA, Savage DCY 2001. Genes encoding bile salt hydrolases and conjugated bile salt transporters in *Lactobacillus johnsonii* 100-100 and other Lactobacillus species. Microbiology 147:3403–3412.

71. Hu N-J, Iwata S, Cameron AD, Drew D. 2011. Crystal structure of a bacterial homologue of the bile acid sodium symporter ASBT. Nature 478:408–411.

844 72. Lu P-H, Li C-C, Chiang Y-W, Liu J-H, Chiang WT, Chao Y-H, Li G-S, Weng S-E, Lin S-Y,
845 Hu N-J. 2021. Dissecting the Conformational Dynamics of the Bile Acid Transporter
846 Homologue ASBTNM. J Mol Biol 433:166764.

847 73. Wang X, Lyu Y, Ji Y, Sun Z, Zhou X. 2021. Substrate binding in the bile acid transporter
848 ASBTYf from *Yersinia frederiksenii*. 1. Acta Cryst D 77:117–125.

849 74. Zhou X, Levin EJ, Pan Y, McCoy JG, Sharma R, Kloss B, Bruni R, Quick M, Zhou M. 2014.
850 Structural basis of the alternating-access mechanism in a bile acid transporter. Nature
851 505:569–573.

852 75. Lord SJ, Velle KB, Mullins RD, Fritz-Laylin LK. 2020. SuperPlots: Communicating
853 reproducibility and variability in cell biology. J Cell Biol 219:e202001064.

854 76. Jenior ML, Leslie JL, Young VB, Schloss PD. *Clostridium difficile* Colonizes Alternative
855 Nutrient Niches during Infection across Distinct Murine Gut Microbiomes. mSystems
856 2:e00063-17.

857 77. Karasawa T, Ikoma S, Yamakawa K, Nakamura S. 1995. A defined growth medium for
858 *Clostridium difficile*. Microbiology 141:371–375.

859 78. Cox J, Hein MY, Luber CA, Paron I, Nagaraj N, Mann M. 2014. Accurate Proteome-wide
860 Label-free Quantification by Delayed Normalization and Maximal Peptide Ratio Extraction,
861 Termed MaxLFQ. Mol Cell Proteomics 13:2513–2526.

862 79. Shen A, Lupardus PJ, Morell M, Ponder EL, Sadaghiani AM, Garcia KC, Bogyo M. 2009.
863 Simplified, enhanced protein purification using an inducible, autoprocessing enzyme tag.
864 PLoS ONE 4.

865

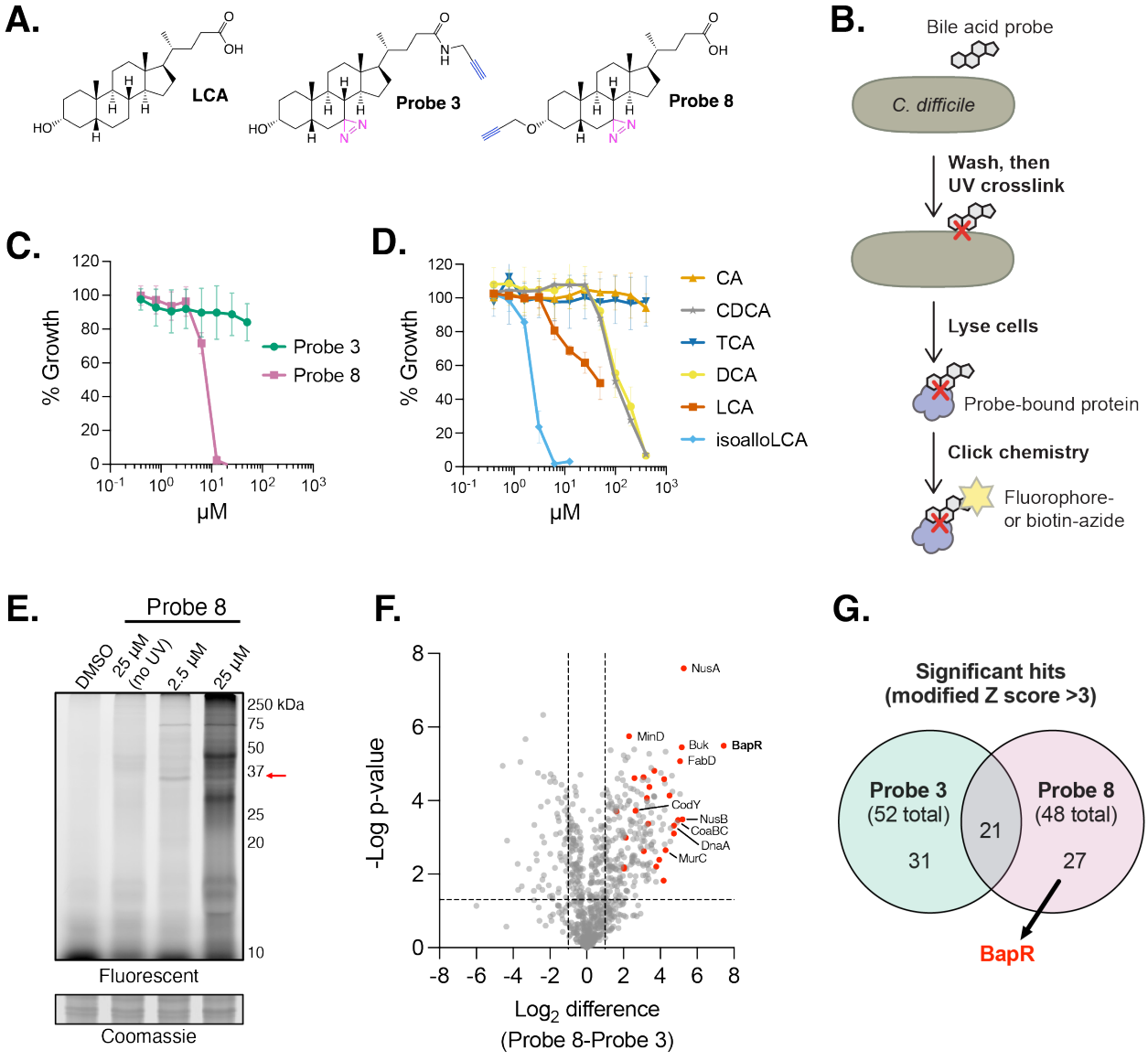

Figure 1. Identification of bile acid binding proteins by chemical proteomics. (**A**) Structures of bile acid probes; diazirine ring for UV crosslinking shown in magenta and terminal alkyne for click chemistry shown in blue. (**B**) Schematic of bile acid probe labeling and detection. (**C**) Inhibition of *C. difficile* growth in broth culture across various concentrations of bile acid probes calculated from OD_{600} after 5 hours of growth; error bars represent SD, n = 4 in two experiments.

875 (**D**) Growth inhibition as in (C) with bile acids; error bars represent SD, n = 4 in two experiments.
876 (**E**) In-gel fluorescent detection of probe labeling as illustrated in (C); cells were treated with probe
877 for 30 minutes during log phase and Coomassie stain serves as a loading control, the gel is
878 representative of three experiments. The red arrow indicates a band approximately the size of
879 BapR. (**F**) Comparison of proteins isolated from *C. difficile* using Probe 8 vs Probe 3 and identified
880 by LC-MS/MS; cells were grown with 10 μM probes for 1 hour during log-phase, dashed lines
881 indicate $p < 0.05$ or 2-fold LFQ intensity difference and significant hits for Probe 8 (modified Z
882 score > 3) are shown in red, n = 3. (**G**) Comparison of hits in each dataset, BapR is a significant
883 hit for Probe 8 but not Probe 3.
884
885
886
887
888
889
890
891

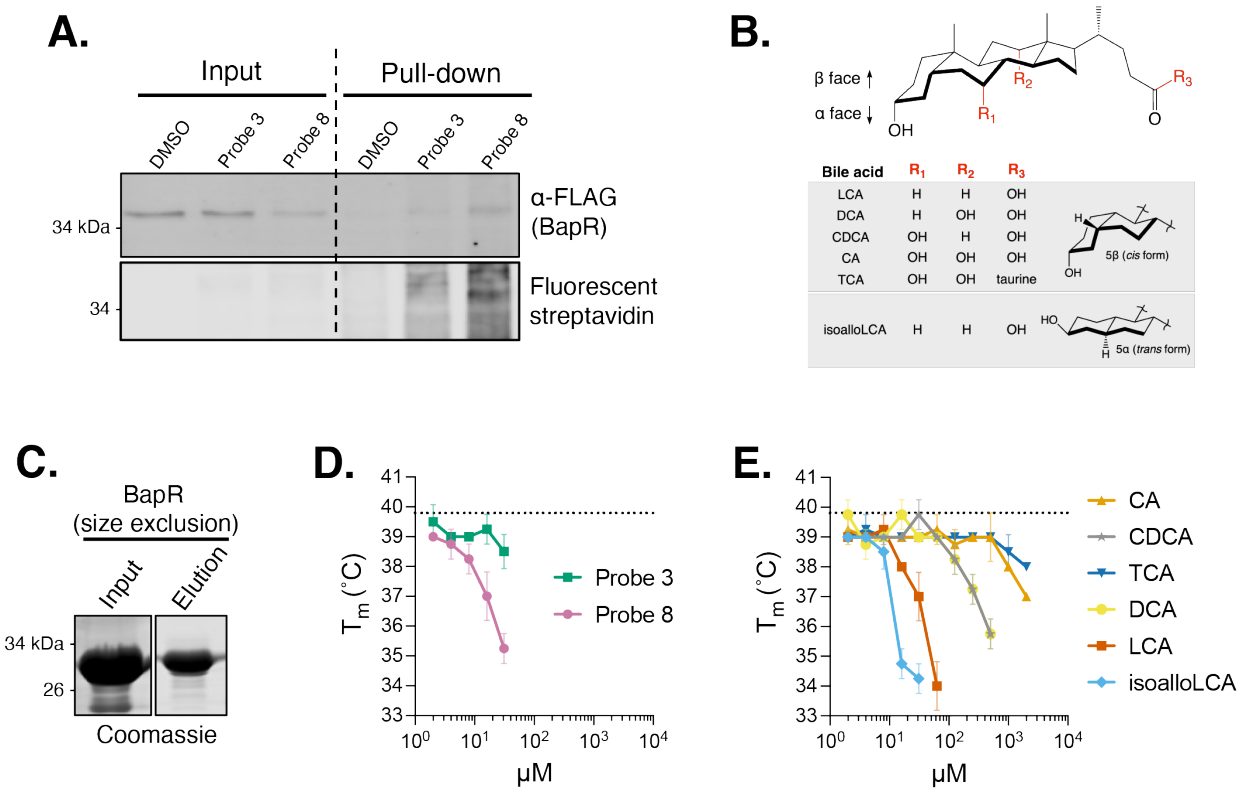

Figure 2. Validation of BapR as a bile acid-binding protein. (**A**) Pull-down of BapR from *C. difficile* using bile acid probes; cells were treated with 10 μM probes for 1 hour during log-phase before following the workflow in Figure 1C with biotin, then streptavidin beads pulled down the probe and BapR if bound. BapR was FLAG-tagged to facilitate its detection. Input samples were taken after the click reaction conjugating biotin to the probe, and fluorescent streptavidin detects presence of the probe. Blot is representative of 3 independent experiments. (**B**) Summarized structures of the bile acids used in this study. (**C**) Size exclusion chromatography of BapR after affinity purification. The gel is representative of 2 independent purifications. (**D**) Thermal shift assay with purified BapR; the melting temperature (T_m) of BapR was assessed using SYPRO Orange dye across a range of bile acid probe concentrations; a change in melting temperature is indicative of binding. Dashed line indicates T_m of BapR in the presence of DMSO vehicle, error bars represent SD, n = 4 with protein from two independent protein purifications. (**E**) Thermal shift assay as in (D) with bile acids.

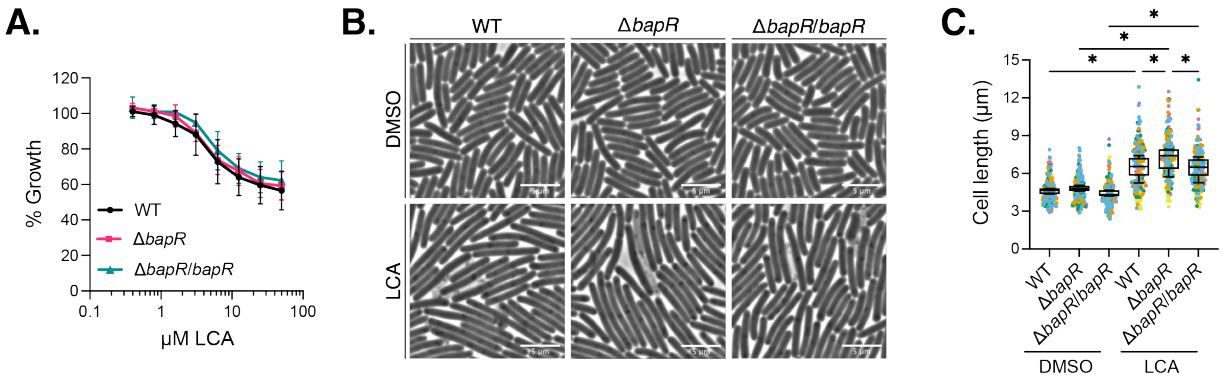

Figure 3. BapR influences cell length in the presence of LCA. (**A**) Inhibition of WT, Δ*bapR*, and Δ*bapR*/*bapR C. difficile* growth in broth culture across various concentrations of LCA calculated from OD_{600} after 5 hours of growth; error bars represent SD, n = 2. (**B**) Phase-contrast images of wildtype (WT) *C. difficile*, Δ*bapR*, and Δ*bapR*/*bapR,* the complement strain carrying *bapR* at an ectopic locus after 3-hour treatment with 20 μM LCA or DMSO vehicle during log-phase; images are representative of 5 independent experiments. (**C**) Measurement of cell length from the experiments in (A); at least 460 cells were measured per strain per condition for each experiment and the length of 35 random cells per experiment are shown (75). Colors represent independent experiments, *p < 0.05 by repeated measures one-way ANOVA with Tukey correction.

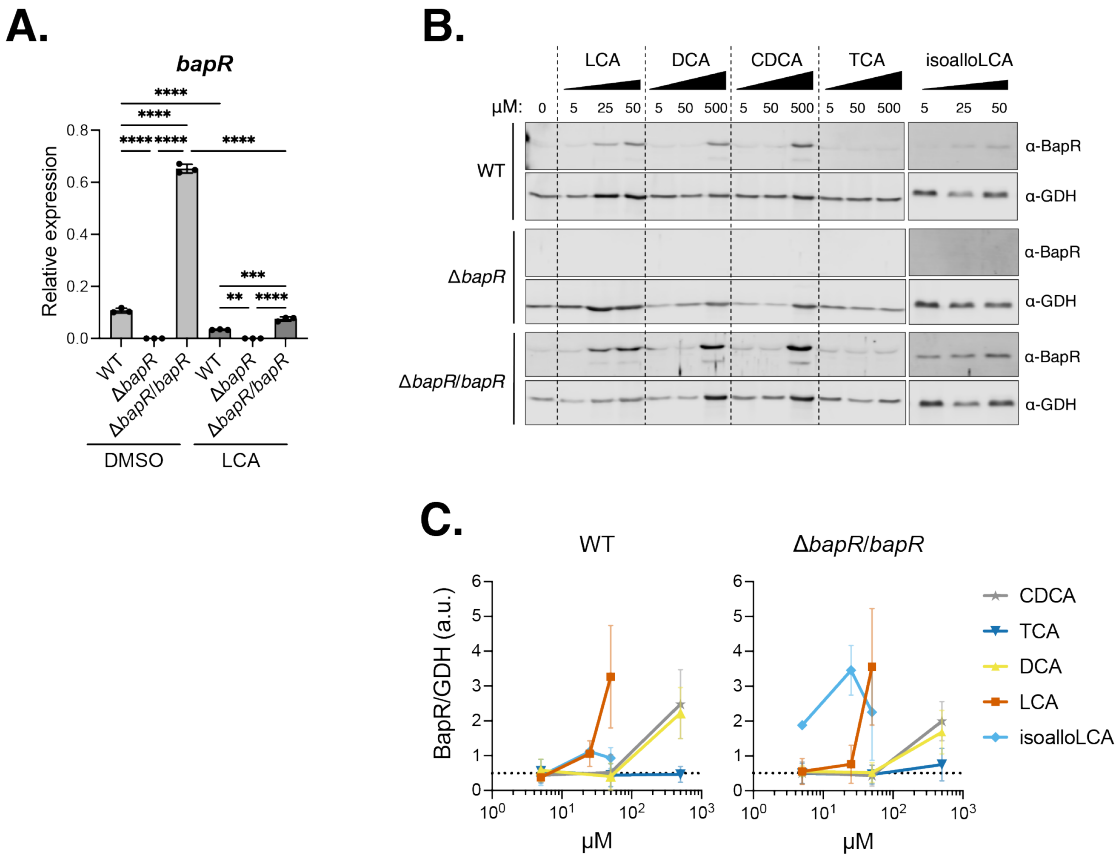

Figure 4. BapR is stabilized by bile acids. (**A**) Expression of *bapR* measured by qRT-PCR after 1-hour exposure to 20 μM LCA or DMSO vehicle; expression is relative to the housekeeping threonyl-tRNA synthetase *thrS* (76). n = 3, **p < 0.01, ***p < 0.001, ****p < 0.0001 by one-way ANOVA with Tukey correction. (**B**) Bile acids were added to log-phase *C. difficile* cultures at the indicated concentrations and samples were taken after 3 hours for Western blotting; glutamate dehydrogenase (GDH) serves as a loading control and blots are representative of 3 biological replicates. (**C**) Quantification of the blots in (A); n = 3.

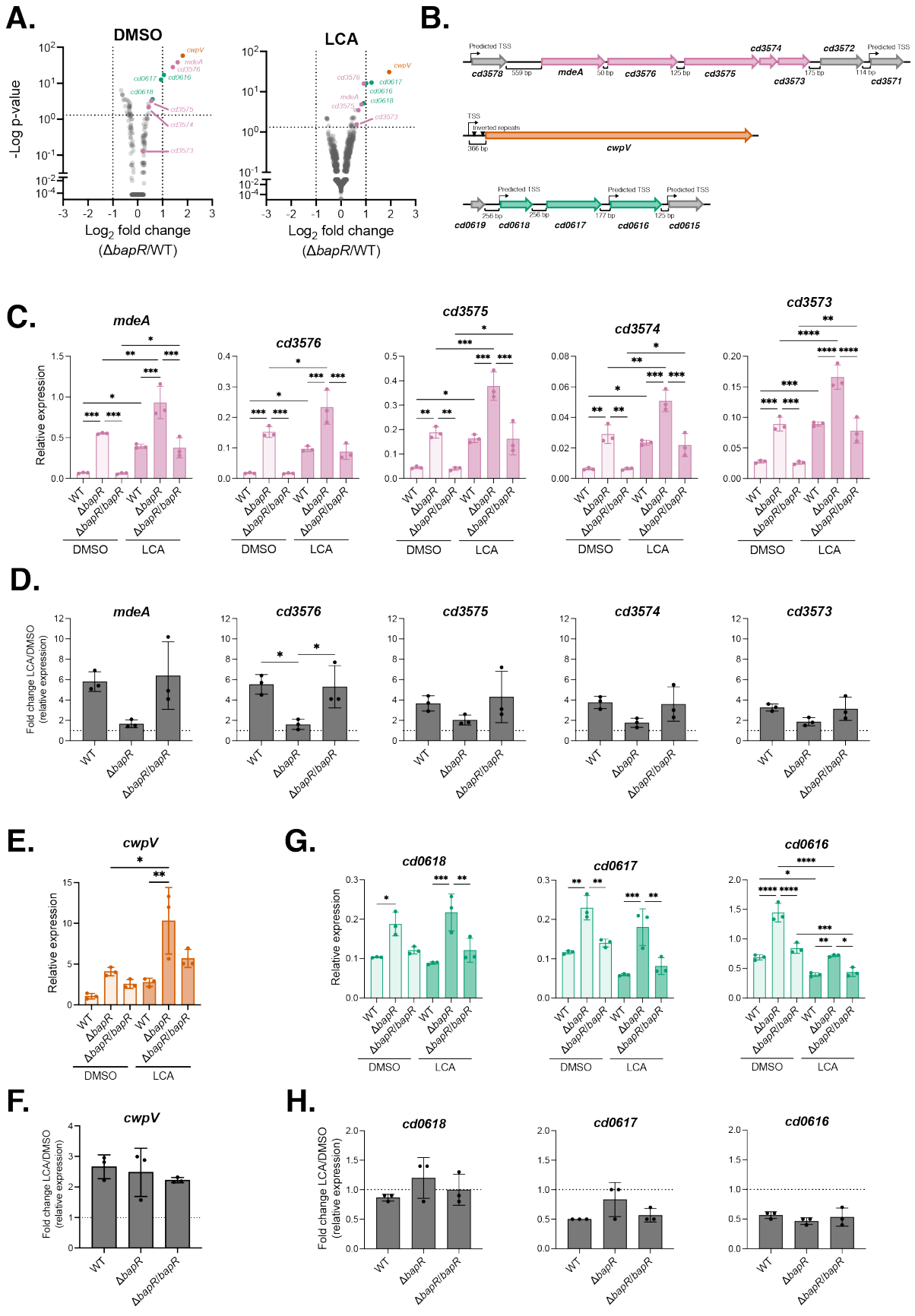

927

928 **Figure 5. Genes regulated by BapR.** (**A**) RNA-seq analysis of WT and Δ*bapR C. difficile* after
929 1-hour treatment with DMSO vehicle or 20 μM LCA during log-phase; dashed lines indicate
930 significance cutoffs at $p < 0.05$ and fold change>2, n = 3. (**B**) Genomic context of hits from (A).
931 (**C**) Expression of the *mdeA* gene cluster measured by qRT-PCR using purified RNA that is
932 distinct from the 1-hour exposure to DMSO or 20 μM LCA used for RNA-seq; expression is relative
933 to *thrS*, n = 3. (**D**) Relative expression data in (C) plotted as fold change LCA over DMSO for each
934 strain. (**E**) Expression of *cwpV* as in (C). (**F**) Fold change LCA/DMSO for *cwpV* as in (D). (**G**)
935 Expression of *cd0618* gene cluster as in (C). (**H**) Fold change LCA/DMSO for *cd0618* gene cluster
936 as in (D). *$p < 0.05$, **$p < 0.01$, ***$p < 0.001$, ****$p < 0.0001$ by one-way ANOVA with Tukey
937 correction.
938
939

940

941

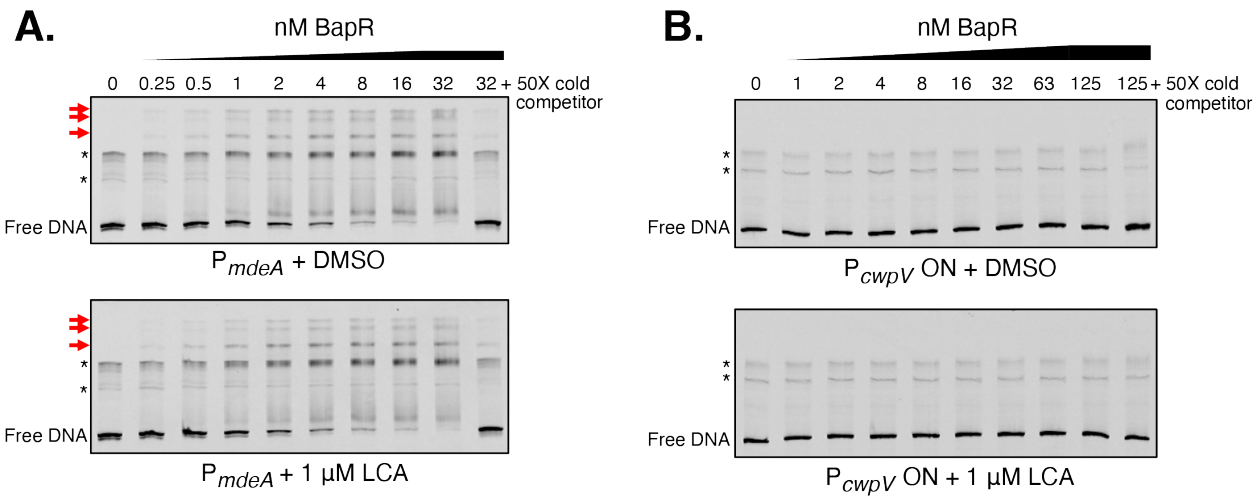

942

943 **Figure 6. BapR directly regulates *mdeA*.** (**A**) Electrophoretic mobility shift assay with purified
944 BapR and a 250 bp DNA fragment comprising the region immediately upstream of the *mdeA* start
945 codon as a putative promoter; 20 fmol 5' IRDye800-labeled promoter fragment per lane, the last
946 lane contains 20 fmol labeled DNA and 1,000 fmol of the same DNA fragment lacking the
947 fluorescent label as a cold competitor. Gel is representative of 3 replicates with protein from 2
948 independent purifications. "Free DNA" indicates unbound DNA and red arrows indicate BapR-
949 bound DNA. Asterisks denote nonspecific bands that likely represent different DNA secondary
950 structures. (**B**) Assay as in (A) with a 356 bp DNA fragment encompassing the *cwpV* promoter in
951 its "on" orientation.

952

953

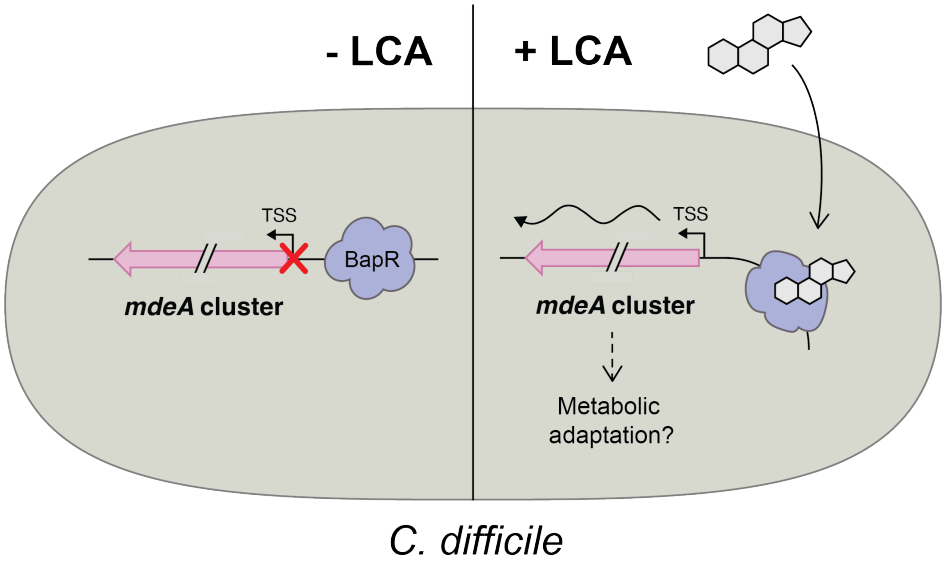

954

955

956 **Figure 7. Model of proposed BapR function.** Consistent with MerR family proteins, BapR is
957 DNA-bound in the absence of LCA and represses gene expression. Upon binding LCA, BapR
958 changes conformation to reorient the promoter and allow transcription, possibly for the purpose
959 of metabolic adaptation.

960